THE JOURNAL OF BIOLOGICAL CHEMISTRY VOL. 288, NO. 34, pp. 24910–24922, August 23, 2013

Structural Basis for the Association of MAP6 Protein with Microtubules and Its Regulation by Calmodulin[S]

Received for publication, January 31, 2013, and in revised form, June 26, 2013 Published, JBC Papers in Press, July 6, 2013, DOI 10.1074/jbc.M113.457267

Julien Lefèvre[‡1], Philippe Savarin[‡2], Pierre Gans[§], Loïc Hamon[‡], Marie-Jeanne Clément[‡], Marie-Odile David[‡], Christophe Bosc[¶], Annie Andrieux[¶], and Patrick A. Curmi[‡3]

From the [‡]Institut National de la Santé et de la Recherche Médicale (INSERM), UMR829; Laboratoire Structure-Activité des Biomolécules Normales et Pathologiques; Université Evry-Val d'Essonne, Evry 91025, France, the [§]Laboratoire de Résonance Magnétique Nucléaire, Institut de Biologie Structurale "Jean-Pierre Ebel," 41 rue Jules Horowitz, Grenoble 38027, France, and the [¶]Team Physiopathologie du Cytosquelette, INSERM U836, Institut des Neurosciences, CEA-iRTSV-GPC, Université Joseph Fourier, Site Santé La Tronche, BP170, 38042 Grenoble Cedex 9, France

Background: Microtubules are cold-sensitive, but some cold-stable microtubules are observed in specific cells due to the presence of MAP6.
Results: Structural data detail how a MAP6 fragment stabilizes microtubules and how calmodulin regulates its activity.
Conclusion: MAP6 may stabilize microtubules by bridging adjacent tubulin heterodimers, an activity sterically hindered by calmodulin.
Significance: This work provides a better understanding of cellular microtubule stabilization and its regulation by calmodulin.

Microtubules are highly dynamic αβ-tubulin polymers. *In vitro* and in living cells, microtubules are most often cold- and nocodazole-sensitive. When present, the MAP6/STOP family of proteins protects microtubules from cold- and nocodazole-induced depolymerization but the molecular and structure determinants by which these proteins stabilize microtubules remain under debate. We show here that a short protein fragment from MAP6-N, which encompasses its Mn1 and Mn2 modules (MAP6(90–177)), recapitulates the function of the full-length MAP6-N protein toward microtubules, *i.e.* its ability to stabilize microtubules *in vitro* and in cultured cells in ice-cold conditions or in the presence of nocodazole. We further show for the first time, using biochemical assays and NMR spectroscopy, that these effects result from the binding of MAP6(90–177) to microtubules with a 1:1 MAP6(90–177):tubulin heterodimer stoichiometry. NMR data demonstrate that the binding of MAP6(90–177) to microtubules involve its two Mn modules but that a single one is also able to interact with microtubules in a closely similar manner. This suggests that the Mn modules represent each a full microtubule binding domain and that MAP6 proteins may stabilize microtubules by bridging tubulin heterodimers from adjacent protofilaments or within a protofilament. Finally, we demonstrate that Ca^{2+}-calmodulin competes with microtubules for MAP6(90–177) binding and that the binding mode of MAP6(90–177) to microtubules and Ca^{2+}-calmodulin involves a common stretch of amino acid residues on the MAP6(90–177) side. This result accounts for the regulation of microtubule stability in cold condition by Ca^{2+}-calmodulin.

In certain cell types such as neurons, fibroblasts, or glial cells, a subpopulation of microtubules (MTs)[4] remains stable in depolymerizing conditions such as exposure to the cold or depolymerizing drugs (1–5). Search for cellular factors responsible for this stabilization led to the discovery of a class of microtubule-associated proteins named MAP6 (also called STOP) (6–8). In mammals, MAP6 isoforms are encoded by a single gene (*map6*) and result from mRNA splicing and alternative promoter use (9–11). The physiological role of MAP6 proteins is not yet fully understood, but phenotypic and cellular analyses of MAP6 null mice indicated that MAP6 proteins are involved in a number of neuronal functions. MAP6 null mice present defects in synaptic plasticity and neurotransmission associated with severe behavioral disorders (12). Interestingly, these disorders can be alleviated by drugs similar to neuroleptics, suggesting that these mice may represent a valuable animal model for the study of schizophrenia (13). In line with these findings, genetic studies have pointed out a possible link between MAP6 and schizophrenia (14), suggesting that *map6* could be considered as a candidate gene that predispose to schizophrenia and thus be used as a potential biomarker for its early detection (15, 16). Besides, MAP6 proteins were also found to be implicated in adult olfactory neurogenesis (17), and MAP6-F (the fibroblastic MAP6 isoform) was proposed to be a temperature sensor that protects MTs from temperature variations in animals during episodes of torpor or hibernation (18).

MAP6-N (the neuronal MAP6 isoform) is the largest MAP6 isoform and is mainly expressed in mature neurons. This 952-residue protein contains several repeated motifs called Mn and Mc modules, which are linked to its ability to stabilize MTs (see Fig. 1*A*) (19). The Mn modules allow MAP6 to protect MTs against cold- and nocodazole-induced depolymerization while

[S] This article contains supplemental Table 1 and Fig. S1.

[1] Recipient of a postdoctoral fellowship from the PRES UniversSud. To whom correspondence may be addressed. Tel.: 33-1-69-47-01-83; E-mail: julien.lefevre@univ-evry.fr.
[2] Present address: Laboratoire CSPBAT (CNRS), UMR 7244, Université Paris 13, Sorbonne Paris Cité, Bobigny 93017, France.
[3] To whom correspondence may be addressed. Tel.: 33-1-69-47-01-87; Fax: 33-1-69-47-02-19; E-mail: pcurmi@univ-evry.fr.

[4] The abbreviations used are: MT, microtubule; AFM, atomic force microscopy; CaM, calmodulin; ITC, isothermal titration calorimetry; MAP6-F, fibroblastic MAP6 isoform; MAP6-N, neuronal MAP6 isoform; STOP, stable tubule only polypeptide.

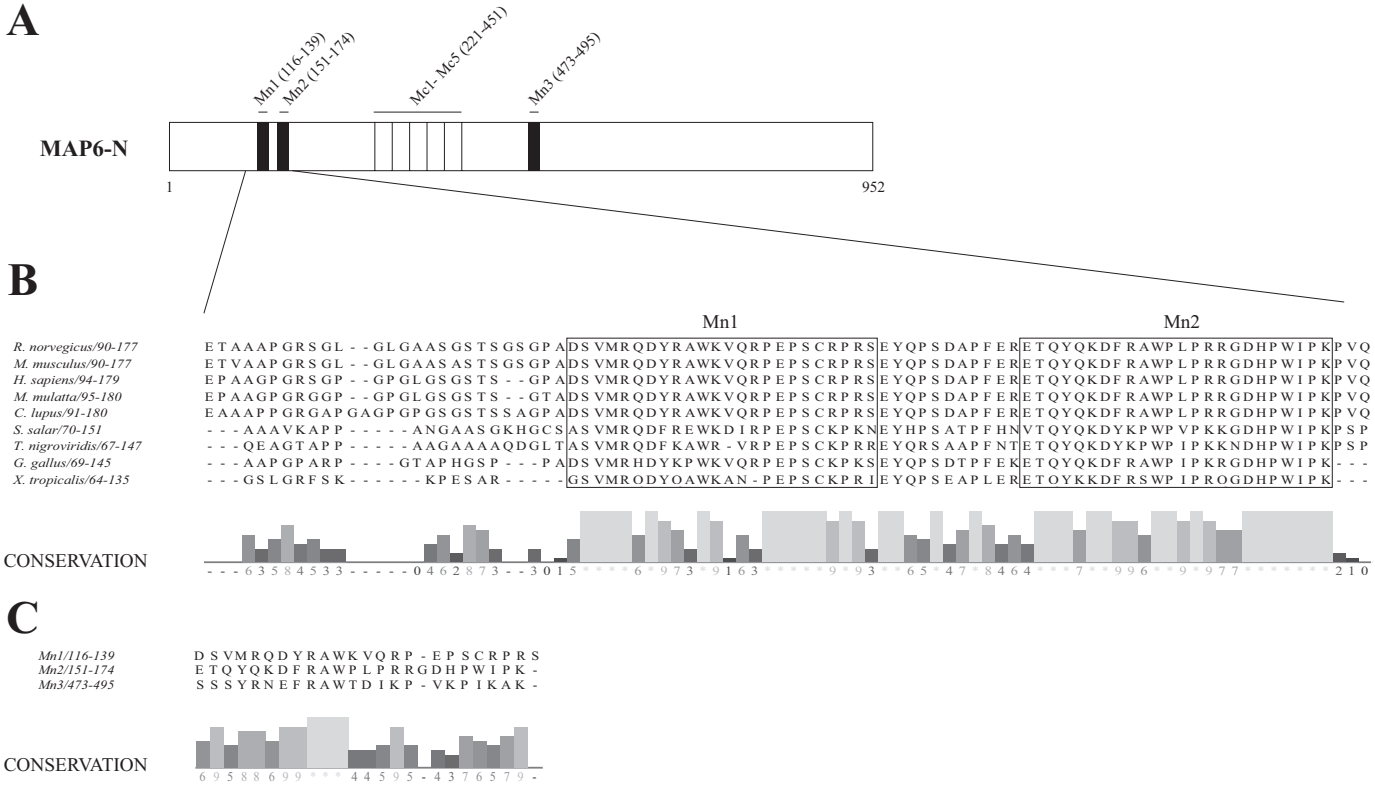

FIGURE 1. **Mn modules from MAP6-N are conserved across species.** *A*, schematic representation of the MAP6-N protein (*Rattus norvegicus*). *B*, sequence alignment of MAP6-N Mn1 and Mn2 modules from different species obtained with the ClustalW2 software (50). Conservation is based on the AMAS method of multiple sequence alignment analysis and reflects the conservation of physico-chemical properties of amino acids (51). Accession numbers are as follows: *R. norvegicus,* NP_058900 (NCBI); *Mus musculus*, NP_001041632 (NCBI); *Homo sapiens*, AAI50255 (GenBank™), *Macaca mulatta* AFJ70456 (GenBank™); *Canis lupus*, XP_534007 (NCBI); *Salmo salar*, NP_001167398 (NCBI); *Tetraodon nigroviridis*, CAF90592 (GenBank™); *Gallus gallus*, NP_990250 (NCBI); *Xenopus tropicalis*, NP_001120222 (NCBI). *C*, sequence alignment of the three Mn modules of MAP6-N (*R. norvegicus*).

the Mc modules permit MAP6 to stabilize MTs in cold condition. MAP6-N contains two consecutive Mn modules in its N-terminal part (Mn1 and Mn2) and an additional one isolated in the middle of its sequence (Mn3). The Mc modules are clustered in the central domain as five highly conserved repetitions organized in tandem. Whereas Mn modules are well conserved across species (see Fig. 1*B*), the homology between Mn1, Mn2 and Mn3 is low, and they share only a few residues (Fig. 1*C*). It is worth noting that the number and the organization of Mn and Mc modules can be different among the MAP6 isoforms, and this may lead to functional variations toward the propensity of MAP6 proteins to stabilize MTs (8, 18, 19). In addition, it was shown that the MT stabilization activity of MAP6 proteins is inhibited by calmodulin (CaM) (20, 21). Accordingly, peptide arrays revealed that MAP6-N possesses several CaM binding sites, some of which being found in the Mn and Mc modules, suggesting that these modules have a dual propensity to interact both with MTs and CaM (19). Very few studies addressed the structural basis of the interaction of MAP6 with MTs and of its interplay with CaM. An NMR study of the interaction between CaM and a peptide model corresponding to the consensus Mc motif showed an unusual interaction mode with a very limited structural impact on the CaM structure (22).

In the present work, we undertook biochemical and structural analyses of the interaction of MAP6-N with MTs and CaM to enlighten the mechanism by which it stabilizes MTs and the mechanisms by which such stabilization is regulated by CaM. As MAP6-N has a high molecular weight, we focused this work on a minimal MAP6-N fragment (residues 90–177, named herein MAP6(90–177)), which recapitulates the MT stabilization and CaM binding properties of MAP6 proteins. We show here that the MAP6(90–177) fragment, which comprises the Mn1 and Mn2 modules, interacts tightly with MTs, and has a powerful MT stabilization activity *in vitro* and in cultured cells. It also interacts with CaM in a Ca^{2+}-dependent manner. Using a combination of biochemical and NMR experiments, we determined at the residue scale the location of its MT and CaM binding sites, and we clearly demonstrated that Ca^{2+}-CaM binding impairs MAP6(90–177) association with MTs probably because the Ca^{2+}-CaM binding sites substantially overlap the MT binding sites. Furthermore, we examined by NMR the structural impact of MAP6(90–177) binding on the Ca^{2+}-CaM structure. The results showed dramatic conformational and dynamical changes of Ca^{2+}-CaM affecting its overall structure which led us to propose a binding mode for Ca^{2+}-CaM on the Mn modules of MAP6 proteins.

EXPERIMENTAL PROCEDURES

Transient Transfection and Immunofluorescence Microscopy—The pCMV-FLAG-MAP6(90–177) plasmid encodes a fusion protein comprising residues 90 to 177 of *Rattus norvegicus* MAP6-N and was constructed by PCR using a derivative of the pSG5-STOP plasmid as template (8). HeLa cells were grown at 37 °C with 5% CO_2 in DMEM containing 5% fetal bovine

serum and 1% penicillin-streptomycin. 5 μg of pCMV-FLAG-MAP6(90–177) plasmid was mixed with 5 μl of Lipofectamine 2000 (Invitrogen) and then diluted in 200 μl of opti-MEM I. This mix was left for 20 min at 20 °C and then added to the HeLa cells culture medium and gently mixed. Cells were returned to the incubator for 4 h at 37 °C, and the medium was replaced with fresh full medium. 48 h post-transfection, cells were either exposed to cold (on ice for 30 min) or to nocodazole (20 μM for 30 min at 37 °C). Cells were then washed twice with PBS and fixed/permeabilized with paraformaldehyde (30 min at 4 °C) and cooled methanol (5 min at −20 °C). After washing, cells were incubated 1 h at 37 °C with the blocking solution (20 mM Tris-HCl, 150 mM NaCl, 0.1% Triton, 2% BSA, 0.1% NaN_3, pH 7.4). The MT network and MAP6(90–177) were revealed by immunofluorescence with E7 anti-α-tubulin mouse antibody (1:3000) and anti-FLAG rabbit antibody (1:160) (Sigma-Aldrich). Cells were washed twice with PBS and incubated with goat anti-mouse (Alexa Fluor 488) and anti-rabbit (Alexa Fluor 594) antibodies. The cells were finally washed with PBS and examined for fluorescence with a Zeiss microscope using a 63×/1.4 numerical aperture objective.

Protein Expression and Purification—The MAP6(90–177) fragment was overexpressed in a recombinant form in fusion with an N-terminal polyhistidine tag using the pET-46 Ek/LIC plasmid (Novagen-Merck, Darmstadt, Germany). After transformation with the pET-46 Ek/LIC plasmid, *E. coli* BL21 DE3* cells (Invitrogen) were grown in LB medium at 37 °C with 0.1 mg/ml ampicillin in a 1-liter flask. For ^{15}N-^{13}C uniform isotopic labeling, transformed bacteria were grown in M9 minimal medium containing 0.6 g/liter 95% $^{15}NH_4Cl$, and 2.2 g/liter 95% ^{13}C-glucose (Cortecnet, Paris, France) as the sole nitrogen and carbon sources, respectively. In all cases, overexpression was induced at $A_{600\ nm} = 0.7$ with 1 mM isopropyl 1-thio-β-D-galactopyranoside for 2 h. Bacteria were pelleted by low speed centrifugation (3,200 × *g*, 10 min) and then resuspended in 10 ml of buffer A (20 mM Tris-HCl, 100 mM NaCl, 1 mM DTT, pH 7.6). After lysis by sonication, the lysate was heated for 25 min at 95 °C and then ultracentrifuged at 4 °C (100,000 × *g* for 1 h). The clarified cell lysate was then loaded on a nickel-nitrilotriacetic acid column (Qiagen, Hilden, Germany) equilibrated with buffer A supplemented with 10 mM imidazole. The proteins were eluted with buffer B (20 mM Tris-HCl, 100 mM NaCl, 1 mM DTT, 300 mM imidazole, pH 7.6). Fractions containing the MAP6(90–177) were combined and concentrated by ultrafiltration (Amicon, 3-kDa cutoff, Millipore) at 4 °C to 0.5 ml and diluted into 4.5 ml buffer C (50 mM MES-KOH, 150 mM NaCl, 1 mM DTT, pH 6.9). The procedure of concentration/dilution was repeated three times with buffer C to eliminate imidazole. Final concentration of MAP6(90–177) was determined by amino acid analysis. The result was used to determine the extinction coefficient of MAP6(90–177) ($\epsilon_{280\ nm} = 2.3 \times 10^4\ M^{-1}\cdot cm^{-1}$). The final yield was ~1 mg/liter of pure protein. The MAP6(90–142) fragment (residues 90–142 of *Rattus norvegicus* MAP6-N) was obtained using the same protocol ($\epsilon_{280\ nm} = 9.2 \times 10^3\ M^{-1}\cdot cm^{-1}$) with a final yield of 3 mg/liter of pure peptide. All of the purification steps were performed in the presence of protease inhibitor mixtures (Roche Applied Science and Halt, Thermo Scientific, Brebières, France) complemented with 0.1 mg/ml tosyl phenylalanine chloromethyl ketone (TPCK) and tosyl lysine chloromethyl ketone (TLCK). CaM from bovine brain was purchased as a lyophilized powder (Sigma-Aldrich). ^{15}N-^{13}C-labeled CaM was expressed and purified according to Bouvier *et al.* (22).

Tubulin was purified from sheep brain using the method of Castoldi and Popov (23) and stored in liquid nitrogen. Before use, an additional cycle of polymerization/depolymerization was performed, and tubulin was resuspended in 50 mM MES-KOH, 4.1 M glycerol, 1 mM $MgCl_2$, 0.5 mM EGTA, pH 6.9. Tubulin concentration was determined by spectrophotometry using an extinction coefficient $\epsilon_{278\ nm} = 1.2 \times 10^5\ M^{-1}\cdot cm^{-1}$.

Binding of MAP6-N Fragments to MTs and MT Stabilization Assays—For MT co-sedimentation assays, tubulin was polymerized for 30 min at 37 °C in 40 mM MES-KOH, 4 mM $MgCl_2$, 1 mM DTT, 1 mM GTP, 2.7 M glycerol, pH 6.9 (buffer P) with stoichiometric amounts of taxol. 0, 5, 15 or 25 μM of taxol-stabilized MTs were then incubated with 20 μM MAP6(90–177) for 15 min at 20 °C. MT pellets were collected by centrifugation (25,000 × *g*, 40 min at 20 °C). To obtain MT binding saturation data, co-sedimentation experiments were performed using a range of concentrations of MAP6(90–177) (0–50 μM) and a fixed amount of taxol-stabilized MTs (10 μM). After 10 min incubation at 20 °C, MT-bound MAP6(90–177) was obtained by centrifugation (25,000 × *g*, 40 min at 20 °C) and estimated by SDS-PAGE using an Odyssey Imaging System (LI-COR Biosciences, Lincoln, NE). The molar binding stoichiometry and dissociation constant (K_d) were determined graphically. The same procedure was used for co-sedimentation assays in the presence of Ca^{2+}-CaM (35 μM taxol-stabilized MTs; 10 μM MAP6(90–177); 0.2 mM $CaCl_2$; 0, 40, and 80 μM CaM; incubation for 5 min at 20 °C). For MT cold stability assays, 25 μM tubulin was polymerized in buffer P for 30 min at 37 °C without (control) or with 20 μM MAP6(90–177). After incubation on ice for 10 min, MT pellets and supernatants were separated by centrifugation (25,000 × *g*, 40 min, 4 °C). To evaluate the influence of Ca^{2+}-CaM on the ability of MAP6(90–177) to stabilize MTs in cold condition, we used the same procedure in the presence of CaM (35 μM MT, 0.5 mM spermine, and 50 μM $CaCl_2$ were first incubated for 10 min at 37 °C with 25 μM MAP6(90–177) alone or in the presence of 100 μM CaM, followed by an incubation for 10 min on ice). The kinetics of MT polymerization were monitored turbidimetrically at 370 nm (1-cm path) in an Ultrospec 3000 spectrophotometer (GE Healthcare) equipped with a temperature controller. 35 μM tubulin was polymerized with 0, 0.35, 3.5, and 35 μM MAP6(90–177) in buffer P at 37 °C. At the steady state, MT destabilization was induced by a cold shock (4 °C) for 2 min. To verify the integrity of the tubulin after the cold treatment, the temperature was then set again at 37 °C. The presence of MTs after the cold shock was examined by atomic force microscopy (AFM) on 10-μl aliquots containing 35 μM MAP6(90–177) and sampled at $t = 30$ min. The samples were deposited on freshly cleaved mica and dried for AFM imaging as described previously (24). All AFM experiments were performed in intermittent mode with a multimode AFM instrument (Digital Instruments, Veeco, Santa Barbara, CA) operating with a Nanoscope

IIIa controller (Digital Instruments). Images were collected at a scan frequency of 1.5 Hz and a resolution of 512 × 512 pixels.

Immobilized CaM-binding Assay—CaM-agarose beads (Sigma-Aldrich) were equilibrated in 50 mM MES-KOH, 1 mM $CaCl_2$, pH 6.9, and incubated with pure MAP6(90–177) for 30 min at 20 °C. Beads were then washed with the same buffer. Flow-through, washes, and CaM bead fractions were analyzed on SDS-PAGE, and the proteins were revealed by Coomassie Blue staining. The Ca^{2+}-dependence of this interaction was tested with calcium-free buffer supplemented with 5 mM EGTA.

Isothermal Titration Calorimetry (ITC)—ITC measurements were performed at 25 °C using an ITC_{200} calorimeter (GE Healthcare). Samples were thoroughly degassed before each titration. Titration and sample solutions were prepared in 20 mM MES-KOH, 50 mM NaCl, 1 mM DTT either with 1 mM $CaCl_2$ or 5 mM EGTA, pH 6.9. Titrations were carried out by injecting 25 consecutive aliquots (1.5 μl) of 200 μM MAP6(90–177) into the ITC cell (0.2 ml) containing 25 μM CaM. A background titration consisting of the identical titration solution but containing only the buffer in the cell was subtracted from each titration to quantify heat produced by sample dilution. The value obtained was subtracted from the heat of reaction to give the effective heat of binding. The resulting titration data were analyzed using the ORIGIN software (MicroCal, Inc.). The molar binding stoichiometry, binding constant ($K_a = 1/K_d$) and binding enthalpy (ΔH) were determined by fitting the binding isotherm to a model with one set of sites. For the fit, no constraint in stoichiometry, K_a and ΔH was introduced. Changes in free energy (ΔG) and in entropy ($T\Delta S$) were calculated from $\Delta G = -RT \ln K_a = \Delta H - T\Delta S$, where R is the gas constant and T is the temperature in Kelvin.

NMR Experiments—MAP6(90–177) and MAP6(90–142) NMR spectra were acquired at 20 °C on a Bruker Avance 600 NMR spectrometer using a cryoprobe. All experiments were performed in 50 mM MES-KOH, 150 mM NaCl, 1 mM DTT, pH 6.9, on 60-μl samples using the MATCH™ system (Cortecnet, Paris, France). Three-dimensional NOESY- and TOCSY-^{1}H-^{15}N HSQC and HNCO, HNCA, HN(CA)CO, CBCA(CO)NH experiments were performed for backbone assignments on a 500 μM ^{15}N- or ^{15}N-^{13}C-labeled MAP6(90–177) sample (25). All spectra were processed with Topspin (version 2.0) and NMRView (26).

^{1}H-^{15}N HSQC experiments were used to characterize the interaction of MAP6(90–177) and MAP6(90–142) with tubulin, taxol-stabilized MTs, apoCaM, Ca^{2+}-CaM, and BSA (negative control). Titration series were performed using ^{15}N-labeled MAP6(90–177) or MAP6(90–142) samples dissolved in 50 mM MES-KOH, 150 mM NaCl, 1 mM DTT, pH 6.9, at 6 °C for tubulin and taxol-stabilized MTs and 20 °C for CaM. Spectra were recorded using 128 × 2048 complex data points in F1 and F2 dimensions with 16 scans per increment. The spectral widths were 1202 and 1500 Hz in the ^{15}N and ^{1}H dimensions, respectively.

A Ca^{2+}-loaded uniformly ^{15}N-^{13}C-labeled CaM sample was prepared at 60 μM in 18 mM Tris-HCl, pH 7.8, and 10% D_2O and studied in a Shigemi tube (Shigemi, Inc., Allison Park, PA). The formation of the MAP6(90–177)·Ca^{2+}-CaM complex was examined on samples by direct addition of different aliquots of a concentrated solution of unlabeled MAP6(90–177) (from a 0.6 mM stock solution) to the ^{15}N-^{13}C-labeled Ca^{2+}-CaM NMR sample to reach 1.5:1 MAP6(90–177):Ca^{2+}-CaM stoichiometry. NMR spectra were acquired at 27 °C on an Agilent VNMRS 800 MHz spectrometer using a cryoprobe. A BEST-TROSY experiment was used as it provided resolution without losing sensitivity compared with ^{1}H-^{15}N HSQC (27). 128 × 930 complex points in the F1 and F2 dimensions were acquired for an experimental time of ~3 h. All data were processed using the NMRPipe software (28). Figures were represented with VMD software (29).

RESULTS

MAP6(90–177) Induces MT Resistance to Cold and Nocodazole in HeLa-cultured Cells—As a prerequisite to biochemical and structural investigation, we verified the functionality of the MAP6(90–177) fragment toward MT stabilization in cultured HeLa cells. HeLa cells are well suited for this type of experiment because they do not endogenously express MAP6 proteins and are devoid of cold-stable and drug-resistant MTs (30). HeLa cells were transfected with the pCMV-FLAG-MAP6(90–177) vector and examined for MT resistance to the cold and nocodazole. Results show that all the transfected cells exhibit a clearly visible MT network, whereas non-transfected cells show a diffuse labeling. Additionally, analysis of the distribution of MAP6(90–177) in transfected cells shows that it colocalizes with the MT network, suggesting that MT stabilization by MAP6(90–177) is direct (Fig. 2). As MAP6(90–177) thus binds to and stabilizes MTs in a cellular context, the investigation of its biochemical and structural properties appears of interest for the characterization of the full length MAP6 proteins.

MAP6(90–177) Binds to MTs and Induces MT Resistance to Cold in Vitro—As a second step, to distinguish between a direct and indirect binding through putative protein partners, we analyzed the association of MAP6(90–177) with MTs *in vitro* using co-sedimentation experiments with taxol-stabilized MTs. In the absence of MT, MAP6(90–177) was not detectable in the pellet, demonstrating that MAP6(90–177) is soluble in these conditions. When MAP6(90–177) was incubated with increasing amounts of MTs, a concentration-dependent MAP6(90–177) binding to MTs was observed (Fig. 3*A*). This result shows that MAP6(90–177) binds directly to MTs. In addition, we found that shearing MTs, which increases the number of MT ends, did not significantly affect MAP6(90–177) binding to MTs (data not shown). To further characterize the MAP6(90–177)/MT interaction, MAP6(90–177) at different concentrations was then incubated with a fixed amount of taxol-stabilized MTs (Fig. 3*B*). MTs were then pelleted, and the MAP6(90–177) content was analyzed by SDS-PAGE and quantified. The results show that the binding of MAP6(90–177) to MTs is saturable with an estimated K_d of 6 μM and a 1:1 MAP6(90–177):tubulin heterodimer stoichiometry.

We then assessed the ability of the MAP6(90–177) fragment to stabilize MTs against cold. After polymerization of tubulin into MTs at 37 °C, MTs were exposed to cold (ice for 10 min) in the absence or presence of MAP6(90–177). SDS-PAGE analysis shows that the amount of MTs in the pellet increases dra-

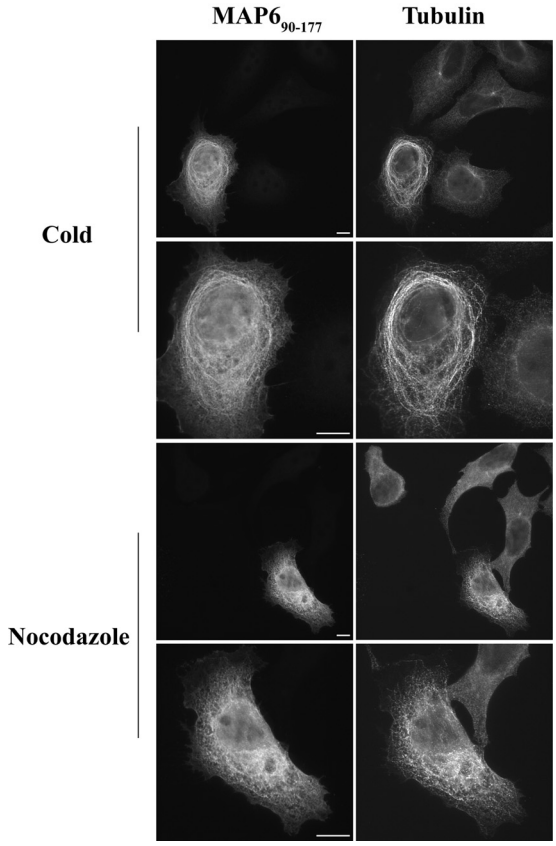

FIGURE 2. **MAP6(90–177) induces MT resistance to cold and nocodazole in HeLa cells.** HeLa cells were transfected with the pCMV-FLAG-MAP6(90–177) plasmid. 48 h after transfection, cells were either exposed to ice or to 20 μM nocodazole for 30 min, fixed/permeabilized, and then stained with anti-tubulin and anti-FLAG antibodies (*scale bar*, 5 μm).

matically in the presence of MAP6(90–177) after cold treatment (Fig. 3*C*). Similar results were observed whether the MAP6(90–177) fragment was mixed to tubulin before polymerization or added to assembled MTs. To confirm that the MAP6(90–177) fragment truly protected MTs from cold depolymerization, we examined the dynamics of MT assembly by turbidimetry at 370 nm (Fig. 3*D*). Results show that the kinetics of tubulin polymerization are very similar in the absence or presence of different concentrations of MAP6(90–177), demonstrating that MAP6(90–177) has no impact on the nucleation and elongation steps. In addition, the steady state turbidity value was also similar in both cases suggesting that no particular supra-assembly of MTs such as bundles were formed in the presence of MAP6(90–177). The cold shock was performed at steady state. In the control condition, it induced a clear MT depolymerization. The effect of this cold shock diminished dramatically in the presence of MAP6(90–177), and a total protection was observed when the MAP6(90–177): tubulin heterodimer ratio reached a value of about 1:1. To ascertain that the macromolecular objects diffusing light during the cold shock in the presence of MAP6(90–177) are really MTs, we performed AFM imaging which shows filamentous structures with length and width in good agreement with MT dimensions (Fig. 3*E*) (31).

Quantification of the MAP6(90–177)/CaM Interaction—It was previously demonstrated that MAP6-N binds to CaM (8) and that Mn modules are implicated in part in this interaction (19). To further investigate such interaction, we examined the binding of MAP6(90–177) to CaM immobilized on beads (Fig. 4*A*). The results show that MAP6(90–177) is able to bind to CaM but only in the presence of $CaCl_2$. Indeed, when the binding experiment was realized with 5 mM EGTA instead of $CaCl_2$, no binding was observed, demonstrating that calcium is necessary for this interaction.

We next carried out ITC experiments to quantify the MAP6(90–177)/CaM interaction. Fig. 4*B* displays the binding isotherm of MAP6(90–177) titration into the Ca^{2+}-CaM solution. The best fit of the integrated isotherm indicated that one MAP6(90–177) binds to two Ca^{2+}-CaM molecules with a K_d value of 0.4 μM (Fig. 4*C*). The same ITC experiment carried out with EGTA in place of $CaCl_2$ showed no detectable interaction.

Identification of MAP6(90–177) Residues Implicated in the Interaction with MTs and Ca^{2+}-CaM—Large amounts of pure and soluble MAP6(90–177) could be obtained from recombinant expression in *Escherichia coli*, which allowed NMR study of MAP6(90–177) interactions with its partners at the residue scale. The ^{1}H-^{15}N HSQC spectrum of MAP6(90–177) in aqueous buffer shows well resolved resonances with a weak dispersion of correlation peaks (<1 ppm and ~20 ppm on the ^{1}H and ^{15}N dimensions, respectively), suggesting that under these conditions, the MAP6(90–177) does not fold into any defined tertiary structure (Fig. 5*A*). NMR assignment of the backbone resonances of MAP6(90–177) was achieved (supplemental Table 1). Analysis of the chemical shifts deviations from random coil values of ^{13}CO and $^{13}C\alpha$ (32) also indicated that MAP6(90–177) does not contain significant secondary structure (Fig. 5*B*). In agreement with this, we observed that during the course of overexpression and purification, the MAP6(90–177) fragment exhibited a high sensitivity to protease degradation together with a high thermostability, properties that are frequently observed for intrinsically unstructured proteins.

To identify MAP6(90–177) residues that mediate MT and Ca^{2+}-CaM interaction, ^{1}H-^{15}N HSQC spectra of free ^{15}N-MAP6(90–177) and bound to unlabeled tubulin, MTs and Ca^{2+}-CaM were recorded (Fig. 6*A*). Because of the large size of these complexes, many ^{1}H-^{15}N cross-peaks of residues implicated in the interaction underwent line broadening and disappeared, which helped us to point them out. Experiments carried out either with tubulin or MTs gave identical results, whereas control experiments performed with BSA showed no modification. A peak by peak analysis using assignment of MAP6(90–177) allowed us to define two MT binding sites delimited by residues 121–138 and 150–175 (Fig. 6*A*). As the C-terminal tail of tubulin is a major binding site for many MT partners, we tested whether this part of tubulin is implicated in the MAP6(90–177)/MT interaction. Co-sedimentation assays were carried out in the presence of an excess of a recombinant tubulin fragment corresponding to the C-terminal tail of α-tubulin (αTub410C) (supplemental Fig. S1) (33). Results show that this αTub410C fragment did not compete with MTs for MAP6(90–177) binding. This result was confirmed by NMR, which showed that the ^{1}H-^{15}N HSQC spectrum of ^{15}N-MAP6(90–177) remained identical in the absence or in the presence of an excess of unlabeled αTub410C (data not shown).

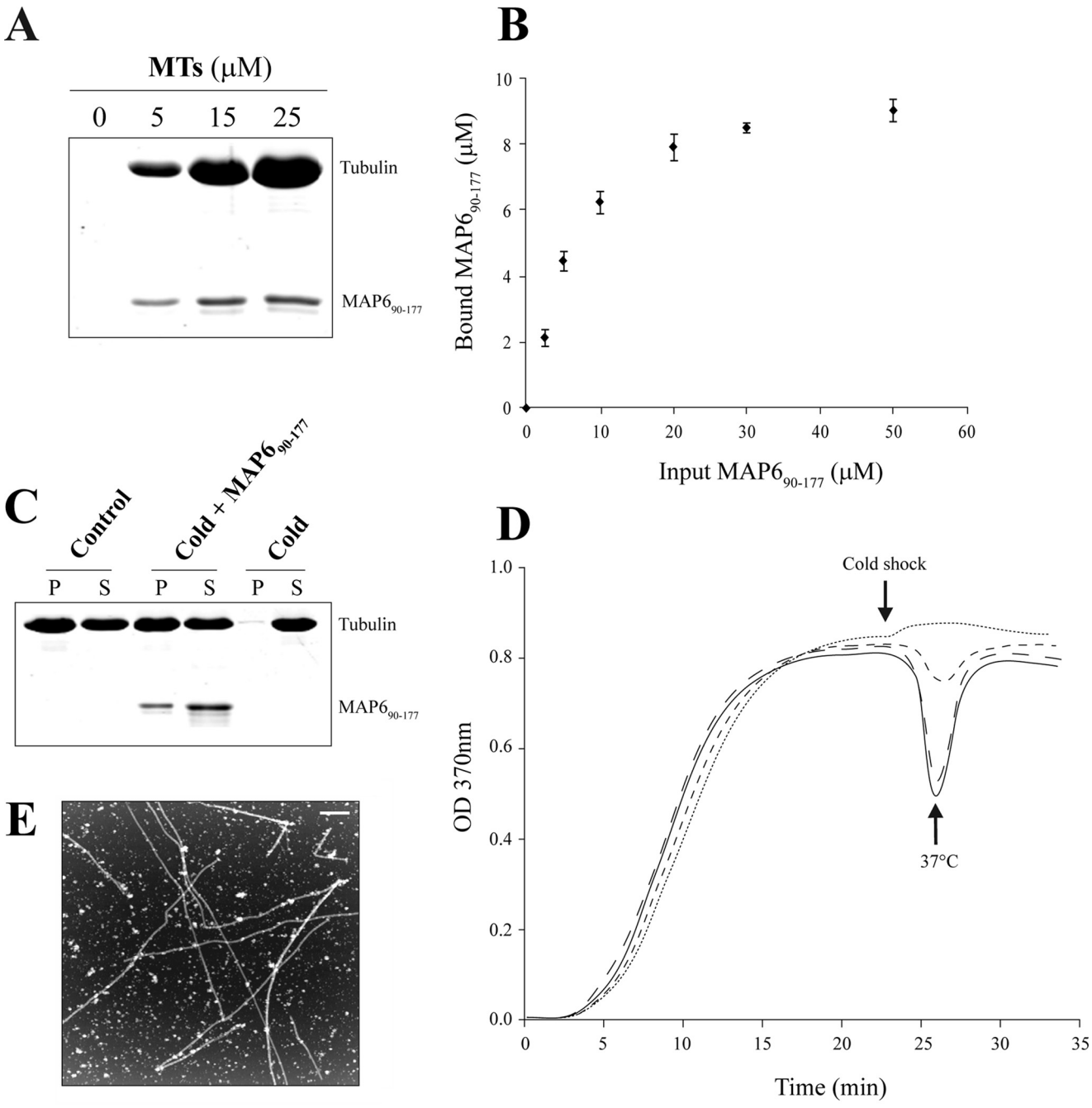

FIGURE 3. **MAP6(90–177) binds *in vitro* to MTs and induces MT resistance to the cold.** *A*, SDS-PAGE analysis of MT co-sedimentation assay. Increasing concentrations of taxol-stabilized MTs were incubated with a fixed amount of MAP6(90–177) (20 μM) and centrifuged. The pellet fractions containing MTs and co-sedimented MAP6(90–177) were run on SDS-PAGE and revealed by Coomassie Blue staining. *B*, saturation curve of MAP6(90–177) fixation to MTs. MAP6(90–177) at different concentrations was incubated with a fixed amount of taxol-stabilized MTs (10 μM). MT-bound MAP6(90–177) was quantified by SDS-PAGE using an Odyssey Imaging System. *Error bars* are from three independent experiments. *C*, SDS-PAGE analysis of MT stabilization assay. 25 μM tubulin was polymerized at 37 °C for 30 min without or with 20 μM MAP6(90–177). After incubation on ice (or 37 °C for the control) for 10 min, MT pellets were collected by centrifugation at 4 °C (or 37 °C for the control) and analyzed by SDS-PAGE and Coomassie Blue staining. *D*, MT formation was assessed by turbidimetry. 35 μM tubulin was polymerized with varying concentrations of MAP6(90–177) at 37 °C: 0 (*black line*), 0.35 (*thick dashed line*), 3.5 (*thin dashed line*), and 35 μM (*dotted line*). MT destabilization was induced by a cold shock at $t = 23$ min (2 min at 4 °C), and the temperature was then set again at 37 °C. *E*, AFM imaging. Image was recorded at $t = 30$ min in the presence of 35 μM MAP6(90–177) (*scale bar*, 1 μm).

We then attempted to locate the Ca^{2+}-CaM binding site on MAP6(90–177) using similar ^{1}H-^{15}N HSQC mapping experiments (Fig. 6*A*). As seen for MTs, Ca^{2+}-CaM binding to ^{15}N-MAP6(90–177) induced line broadening due to the large size of the complex. The mapping of the Ca^{2+}-CaM binding site points out two regions delimited by residues 121–137 and 151–176, which are very similar to those that participate to the binding of MTs. Surprisingly, this suggests a common binding mode for MTs and Ca^{2+}-CaM. Finally, the binding of MAP6(90–177) to Ca^{2+}-CaM could be reversed with EGTA confirming again the Ca^{2+} dependence of the MAP6(90–177)/CaM interaction (data not shown).

We then examined by competition experiments whether Ca^{2+}-CaM could impair MAP6(90–177) binding to MTs (Fig.

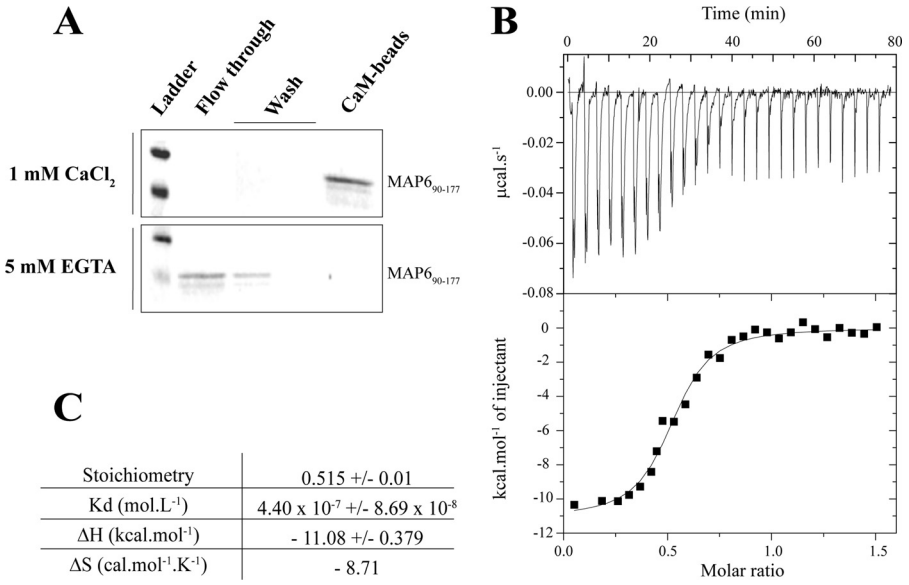

FIGURE 4. **MAP6(90–177) interacts with Ca^{2+}-CaM (K_d = 0.4 µM).** *A*, MAP6(90–177) binds only to the holoform of CaM. MAP6(90–177) was incubated with CaM-agarose beads in the presence or absence of Ca^{2+}. Beads were then washed and flow-through, washes, and CaM bead fractions were analyzed on SDS-PAGE and revealed by Coomassie Blue staining. *B*, ITC analysis of the interaction of MAP6(90–177) with Ca^{2+}-CaM. Heat signal is shown (*top*) with the binding isotherm derived from this signal (*bottom*). *C*, parameters obtained from the best fit.

6*B*). Taxol-stabilized MTs were incubated in the presence of a fixed amount of MAP6(90–177) and increasing concentrations of Ca^{2+}-CaM. Free and MT-bound MAP6(90–177) were then separated by centrifugation and analyzed by SDS-PAGE and Coomassie Blue staining. Results indicate a progressive displacement of MAP6(90–177) from pellet to supernatant as the concentration of Ca^{2+}-CaM increases. Hence, it appears that MTs and Ca^{2+}-CaM bind to MAP6(90–177) in a mutually exclusive manner. This competition was confirmed in functional assays in which the protective effect of MAP6(90–177) for MT cold depolymerization was tested in the presence of Ca^{2+}-CaM (Fig. 6*C*). In this experiment, Ca^{2+} was required to obtain the holo-form of CaM. However, due to the destabilizing effect of Ca^{2+} on MTs, experiments were performed in the presence of excess of spermine, which acts as a Ca^{2+}-competitive inhibitor for MT binding (33). Polymerized MTs were incubated on ice alone (control, the *two left lanes*) or with MAP6(90–177) (the *two middle lanes*) or with MAP6(90–177) and Ca^{2+}-CaM (the *two right lanes*). Results show clearly that MAP6(90–177) no longer protects MTs in the presence of Ca^{2+}-CaM.

Binding of MAP6(90–177) to Ca^{2+}-CaM Induces Large Conformational Changes of the Ca^{2+}-CaM Structure—To study the structural impact of MAP6(90–177) binding on the Ca^{2+}-CaM structure, we carried out NMR experiments with purified and ^{15}N-^{13}C-labeled Ca^{2+}-CaM. BEST-TROSY spectra of ^{15}N-^{13}C-Ca^{2+}-CaM in the absence and presence of unlabeled MAP6(90–177) were recorded (Fig. 7*A*). The addition of MAP6(90–177) to Ca^{2+}-CaM resulted in very large changes of the spectrum profile of Ca^{2+}-CaM with modifications of the peaks number and of the chemical shifts distribution. Residues affected by this interaction are reported on the CaM sequence and on a crystallographic structure of Ca^{2+}-CaM (Fig. 7, *B* and *C*) (34). Results show that the perturbations are found mostly in the N-terminal domain and in the central α-helix of Ca^{2+}-CaM. Indeed, NMR mapping points out a first stretch in the N-terminal domain (residues 13–39) and a second long stretch comprising the end of the N-terminal domain and more than half of the central α helix (residues 49–80). The C-terminal domain is affected but in a lesser extent. Together, these observations indicate that the binding of MAP6(90–177) induces wide range conformational and dynamical changes in the Ca^{2+}-CaM structure, implicating mostly its N-terminal domain and the central α-helix.

MTs and Ca^{2+}-CaM Compete for the Same Binding Site on the Mn1 Module—We finally examined the possibility that a single Mn module could interact with MTs and Ca^{2+}-CaM. To that end, we overexpressed and purified a 53-amino acid residue fragment encompassing the N-terminal part and the Mn1 module of MAP6(90–177) (MAP6-N residues 90–142, named herein MAP6(90–142)). We observed that the ^{1}H-^{15}N HSQC spectrum of MAP6(90–142) superimposes very well with that of the MAP6(90–177) fragment, which strongly facilitated its assignment. When the MAP6(90–142) fragment was studied in the presence of tubulin or MTs, we observed on its ^{1}H-^{15}N HSQC spectrum (Fig. 8*A*) line broadening responsible for the disappearance of some peaks corresponding to the stretch of residues 121–138 with the exception of Cys-135. (Fig. 8*B*). Interestingly, the ^{1}H-^{15}N HSQC spectrum of MAP6(90–142) acquired in the presence of Ca^{2+}-CaM (Fig. 8*A*) gave very close results with line broadening and disappearance of peaks corresponding to residue Val-118 and of the stretch 121–138 except for Gln-129 and Ser-134 (Fig. 8*B*). Hence, these results show that the Mn1 module, when considered isolated from the other Mn modules, is able to bind to both MTs and Ca^{2+}-CaM in a similar manner.

DISCUSSION

MAP6(90–177) Binds and Stabilizes MTs—The aim of this work was to better understand the molecular mechanisms

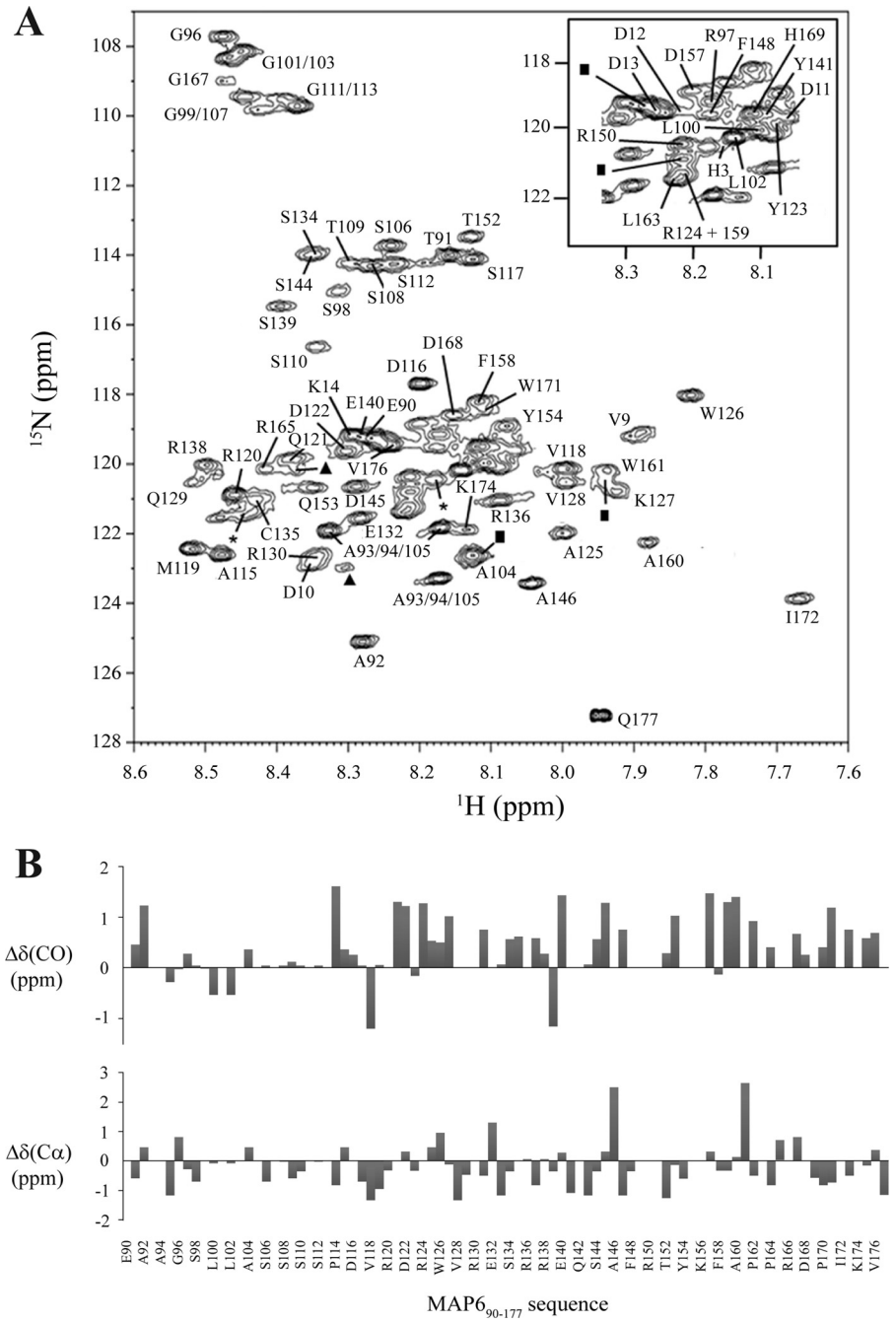

FIGURE 5. **Structural analysis of MAP6(90–177).** *A*, assigned MAP6(90–177) ^{1}H-^{15}N HSQC spectrum in 50 mM MES-KOH, 150 mM NaCl, 1 mM DTT, pH 6.9, at 20 °C. Some indeterminations remained for residues marked with *triangles* (Glu-151 or Arg-166), *stars* (Lys-156), and *rectangles* (Gln-142, Glu-149, or Gln-155). *B*, corresponding secondary chemical shifts for ^{13}CO and ^{13}Cα illustrating the absence of secondary structure.

underlying the stabilization of MTs by MAP6 and its regulation by CaM using biochemical and structural investigations. To that end, we took advantage of a MAP6-N fragment encompassing its Mn1 and Mn2 modules, which recapitulates the functional properties of the full-length protein. As a first step, we studied the interaction between MAP6(90–177) and MTs. Using co-sedimentation assays, we found that MAP6(90–177) interacts with MTs with an apparent K_d value of ~6 μM and a 1:1 MAP6(90–177):tubulin heterodimer stoichiometry (Fig. 3*B*). To the best of our knowledge, this is the first report on a K_d value regarding the interaction of Mn modules with MTs. Delphin *et al.* (18) reported a K_d value of ~70 nM for the interaction between the Mc domain of MAP6-F and MTs. The lower apparent affinity observed here for MAP6(90–177) may be related to the fact that this fragment contains only two Mn modules, whereas the Mc domain contains five Mc modules. This suggests that the binding of MAP6 to MTs may be cooperative. Co-sedimentation assays (supplemental Fig. S1) and NMR experiments (data not shown) using a α-tubulin C-terminal fragment (αTub410C, residues 410–451 from α_{1a}-tubulin (33)) indicated that this part of tubulin is not sufficient for the interaction with MAP6(90–177). This agrees with previous

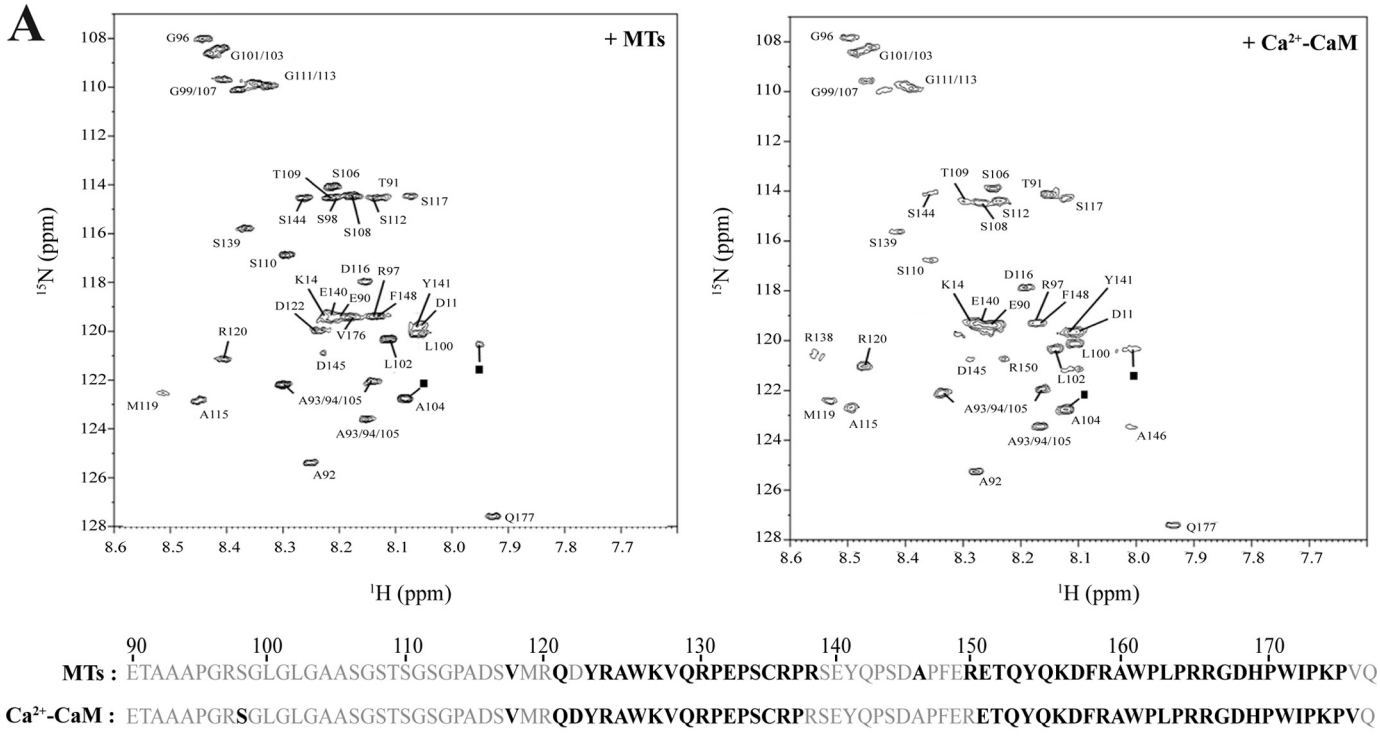

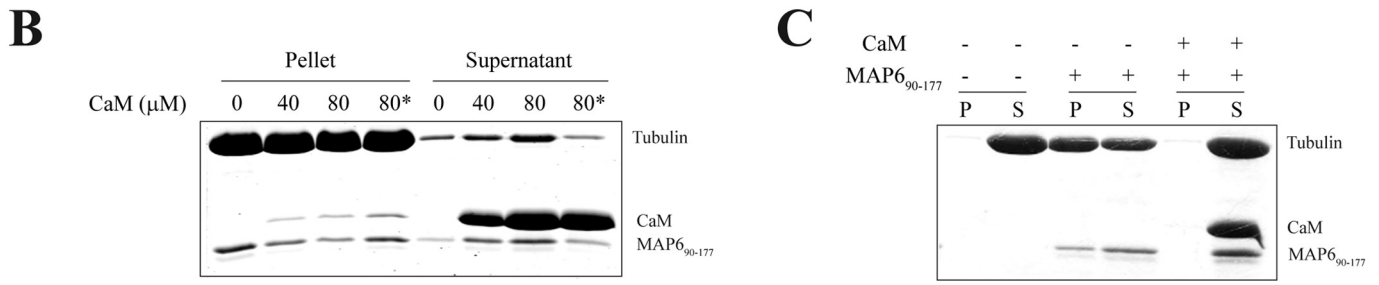

FIGURE 6. **MTs and Ca^{2+}-CaM compete for the same binding site on MAP6(90–177).** *A*, NMR analysis of MAP6(90–177)/MT and MAP6(90–177)/Ca^{2+}-CaM interactions. ^{1}H-^{15}N HSQC spectra of ^{15}N-labeled MAP6(90–177)/MT (molar ratio of 1:2, 6 °C) and ^{15}N-labeled MAP6(90–177)·Ca^{2+}-CaM (molar ratio 1:3, 20 °C) complexes. The MAP6(90–177) residues implicated in the binding of MTs and Ca^{2+}-CaM are highlighted in *boldface* (proline residues lying in or around the sequences were arbitrarily included). *B*, Ca^{2+}-CaM competes with MTs for MAP6(90–177) binding. 35 μM taxol-stabilized MTs were incubated with 10 μM MAP6(90–177), 0.2 mM $CaCl_2$, and varying concentrations of CaM for 5 min at 20 °C. After centrifugation, pellet and supernatant contents were analyzed by SDS-PAGE and Coomassie Blue staining. *Asterisks* correspond to experiments where 0.2 mM $CaCl_2$ was replaced by 0.5 mM EGTA. *C*, Ca^{2+}-CaM inhibits the protective effect of MAP6(90–177) on MTs. 35 μM tubulin was polymerized in the presence of 0.5 mM spermine to counteract the negative effects of Ca^{2+} on MTs. After addition of 50 μM $CaCl_2$, polymerized MTs were incubated on ice for 10 min alone (control, the *two left lanes*) or with 25 μM MAP6(90–177) (the *two middle lanes*) and 100 μM CaM (the *two right lanes*). Pellets and supernatants contents were analyzed by SDS-PAGE and Coomassie Blue staining.

report showing that, unlike other MAPs, MAP6 can bind significantly to any tubulin isoform whatever its degree of C-terminal modification by polyglutamylation (35).

We observed that the stabilization of MTs against cold and nocodazole by MAP6(90–177) does not induce MT aggregates or bundles in contrast to what was observed with full-length MAP6-N by immunofluorescence microscopy (7). In the latter case, the formation of MT bundles may be due either to the presence of multiple Mn and Mc repeats or to a possible multimerization of the protein via stretches of amino acid residues that are located outside of the MAP6(90–177) region. We next mapped the MAP6(90–177) interaction with MTs to two MAP6(90–177) binding sites defined by residues 121–138 and 150–175, which correlate strongly with Mn1 and Mn2 modules, respectively (19). Interestingly, NMR data show that a single Mn module (MAP6(90–142)) can still interact with MTs, suggesting that each Mn module in MAP6 may serve as anchor point for MT binding. Accordingly, each Mn repeat may recognize a conserved binding motif located on α- and β-tubulin. From a structural point of view, MT stabilization by MAP6(90–177) is thus likely to occur through the reinforcement of the longitudinal contacts between tubulin heterodimers within a protofilament as seen for Tau (36) or lateral contacts between adjacent tubulin heterodimers, preventing protofilament separation similar to the stabilization mode of doublecortin (37). In addition, we cannot exclude that MAP6(90–177) may also stabilize MTs by preventing cold- or nocodazole-induced conformational changes in tubulin by a more complex mechanism.

Association of MAP6(90–177) with MTs Is Regulated by Ca^{2+}-CaM—Biochemical and ITC experiments showed that MAP6(90–177) binds to CaM in a Ca^{2+}-dependent manner with a K_d value of 0.4 μM and a 1:2 MAP6(90–177):Ca^{2+}-CaM stoichiometry (Fig. 4). This K_d value lies in the range of that previously reported for MAP6-F/Ca^{2+}-CaM ($K_d \sim$ 1.7 and 8.1 μM) (19) and

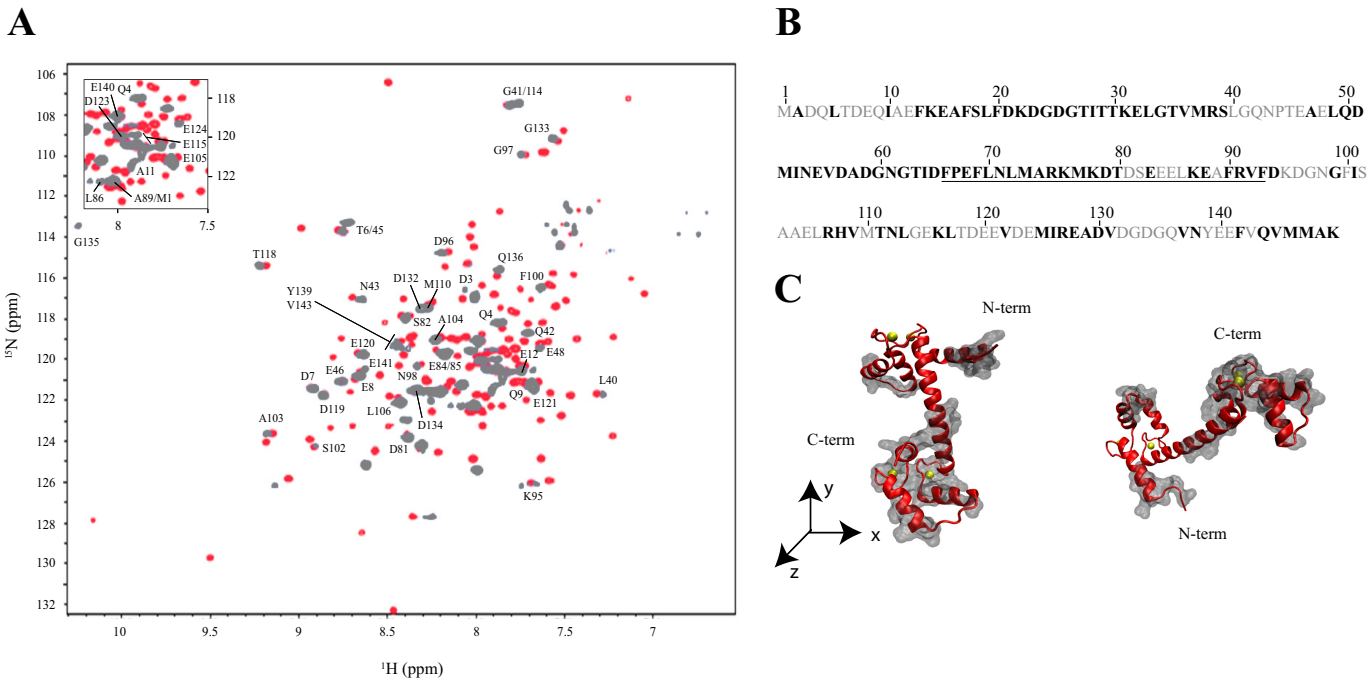

FIGURE 7. **Ca^{2+}-CaM undergoes large conformational changes when in interaction with MAP6(90–177).** *A*, BEST-TROSY spectra superposition of ^{15}N-^{13}C-labeled Ca^{2+}-CaM in the absence (*red*) and presence of MAP6(90–177) (0.5:1 MAP6(90–177):Ca^{2+}-CaM molar ratio) (*gray*). Residues that are not significantly affected by the interaction (no line broadening nor significant chemical shift perturbation $(((\Delta\delta^{1}H)^2 + (\Delta\delta^{15}N/6.5)^2)^{1/2} < 0.09$ ppm (52)) are labeled. *B*, sequence of CaM showing the residues affected by the interaction (*boldface* type). The proline Pro-67 residue was arbitrarily included. The central α-helix separating the N- and C-terminal domains of CaM is *underlined*. *C*, spatial representations of the Ca^{2+}-CaM structure (Protein Data Bank code 1OSA). The image on the *right* was obtained after a 180° rotation around the *x* axis and a 90° rotation around the *z* axis. Residues that are not significantly affected by the interaction are rendered as *gray rigid blocks*. *Yellow spheres*, Ca^{2+} ions.

Mc/Ca^{2+}-CaM ($K_d \sim 1.5$ and 3.9 μM) interactions (22, 38). Such an affinity is compatible with a physiological interaction of Ca^{2+}-CaM with MAP6 for instance after a transient rise in cytoplasmic [Ca^{2+}]. Investigation of MAP6(90–177)/Ca^{2+}-CaM interaction by NMR pointed out two MAP6(90–177) regions (121–137 and 151–176), which are nearly identical to the MAP6(90–177)/MT binding sites. This suggests that Ca^{2+}-CaM may compete with MTs for MAP6(90–177) binding. In agreement with this hypothesis, we demonstrated for the first time using co-sedimentation assays that Ca^{2+}-CaM is responsible for a stoichiometric inhibition of MAP6(90–177) binding to MTs, resulting in a loss of MT stabilization. Altogether, these observations suggest that the regulation of MAP6 binding to MTs by Ca^{2+}-CaM is a dynamic process rapidly modulated by the Ca^{2+} charge state of CaM. A similar mechanism was proposed for Tau in the flip-flop model (39). Finally, this part of MAP6-N also comprises Ser-139, which can be phosphorylated by the Ca^{2+}-calmodulin-dependent protein kinase II, which triggers the translocation of MAP6 from MTs to actin (40). Interestingly, this kind of regulation has already been observed for the microtubule-associated protein p35, which is also regulated by site-specific phosphorylations and Ca^{2+}-CaM with MT overlapping binding sites (41). Similar mechanisms of CaM regulation were again suggested for Tau (42–44).

Impact of MAP6(90–177) on Ca^{2+}-CaM Structure, Implication for the Binding Mode—Previous NMR, infrared spectroscopy and differential scanning calorimetry investigations on the interaction of Ca^{2+}-CaM with a model peptide corresponding to a single Mc motif revealed an unusual binding mode. Indeed, these studies showed that the Mc peptide interacts with the C-terminal domain of CaM, leaving it in an extended conformation with no significant structural change (22, 38). The present data provide strong evidences that the binding mode of MAP6(90–177) to Ca^{2+}-CaM is distinct from that previously observed with Mc modules. However, the present NMR data show that the binding of MAP6(90–177) to Ca^{2+}-CaM produces large structural and dynamical changes in Ca^{2+}-CaM. Interestingly, sequence analysis of the two sites of MAP6(90–177) that interact with Ca^{2+}-CaM suggests that they belong to the 1-5-10 class of canonical CaM-binding motifs found in several CaM-regulated proteins such as Ca^{2+}-calmodulin-dependent protein kinase II and synapsin I (Fig. 9) (45, 46). This class refers to a group of Ca^{2+}-CaM partners whose key hydrophobic bulky residues are spaced by eight residues with an additional anchoring residue in the middle. Upon binding, both Ca^{2+}-CaM and the target peptide motif undergo large conformational rearrangements. The canonical CaM-binding motif adopts an α-helical conformation and the two domains of CaM wraps around it, enclosing it in a hydrophobic channel within the globular core. The data obtained here on MAP6(90–177)/Ca^{2+}-CaM interaction argue for a similar binding mode: (i) Ca^{2+} is required for MAP6(90–177) binding, a fact that is systematically observed with this type of binding mode; (ii) large structural modifications of the Ca^{2+}-CaM structure are observed affecting its two domains and its central flexible helix; and (iii) the secondary structure prediction of MAP6(90–177) show that residues 117–125 and 148–158 may fold into α-helices. These stretches overlap the 1-5-10 motifs of MAP6(90–177), and it is possible that they locally fold when in complex

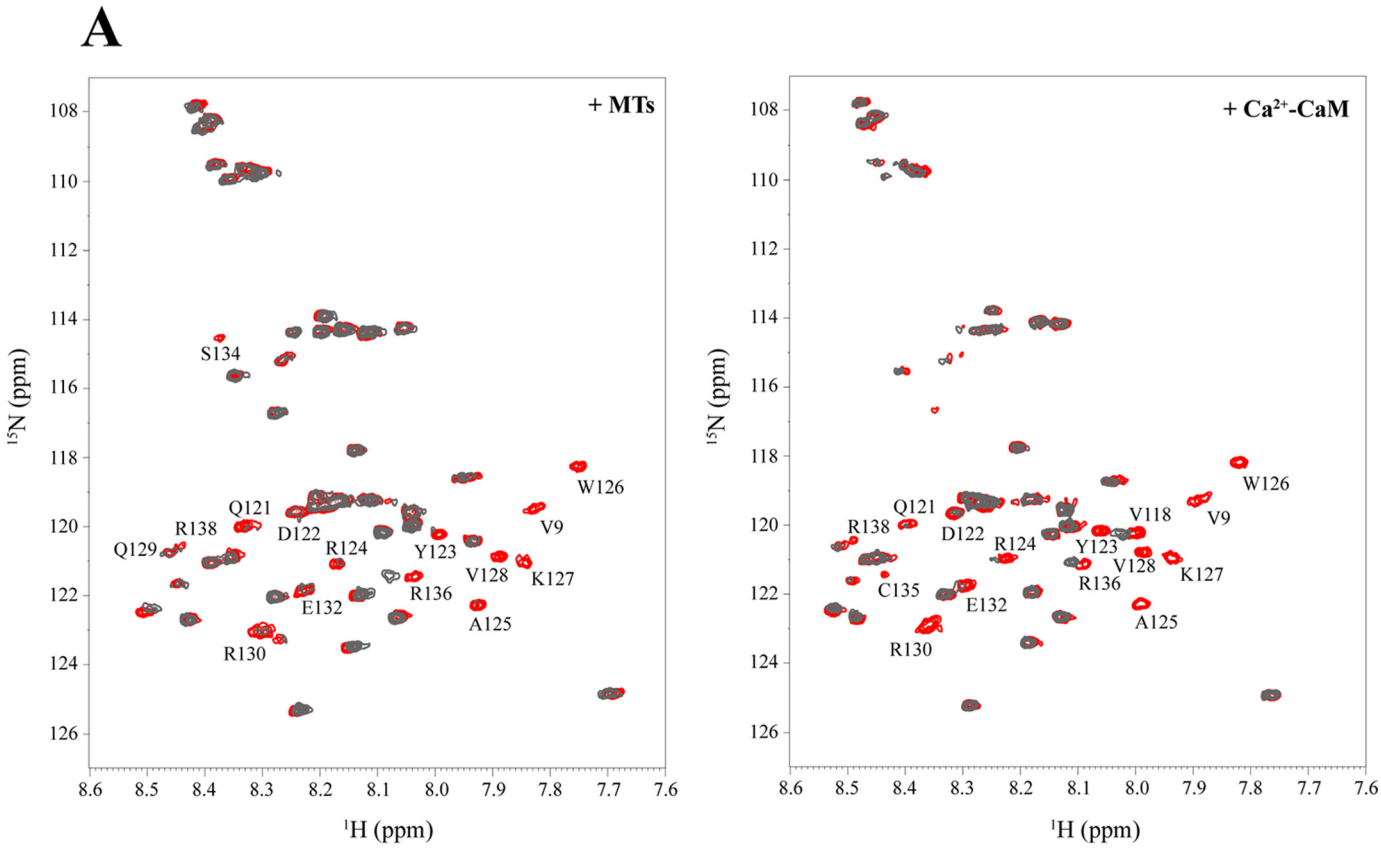

FIGURE 8. **The Mn1 module of MAP6-N (residues 90–142, MAP6(90–142)) interacts with MTs and Ca^{2+}-CaM.** *A*, NMR analysis of MAP6(90–142)/MT and MAP6(90–142)/Ca^{2+}-CaM interactions. ^{1}H-^{15}N HSQC spectra of ^{15}N-labeled MAP6(90–142)·MT and ^{15}N-labeled MAP6(90–142)·Ca^{2+}-CaM complexes (1:1 molar ratio at 6 °C and 1:3 molar ratio at 20 °C, respectively). *B*, residues implicated in the binding of MTs and Ca^{2+}-CaM are highlighted in *boldface* type in the MAP6(90–142) sequence (proline residues lying in the sequences were arbitrarily included).

	1				5					10		
1-5-10 motif	-	-	-	Φ	-	-	-	Φ	-	-	-	-	Φ	-	-
CaMKII/101-115	R	R	K	L	K	G	A	I	L	T	T	M	L	A	T
PI3Kγ/679-693	R	F	L	L	K	R	G	L	R	N	K	R	I	G	H
Cathelicidin-4/129-143	S	V	I	L	P	W	K	W	P	W	W	P	W	R	R
Synapsin I/123-137	H	T	D	W	A	K	Y	F	K	G	K	K	I	H	G
MAP6-N/116-130	D	S	V	M	R	Q	D	Y	R	A	W	K	V	Q	R
MAP6-N/151-165	E	T	Q	Y	Q	K	D	F	R	A	W	P	L	P	R

FIGURE 9. **CaM 1-5-10 binding motif alignment.** Sequence alignment of 1-5-10 class motifs from selected CaM-binding partners. The Ca^{2+}-CaM-interacting region delimited by NMR MAP6(90–177) comprises two canonical CaM binding motifs belonging to the 1-5-10 class. *CaMKII*, CaM kinase II.

with Ca^{2+}-CaM. It is worthy to note that neither the Mc modules nor the Mn3 module of MAP6 (which bind to Ca^{2+}-CaM) contain such a 1-5-10 motif. This may explain previous reports showing an unusual binding mode for these CaM-binding sites (22).[5] Interestingly, some 1-5-10 motifs were shown to be implicated both in Ca^{2+}-CaM and actin binding (47–49), and MAP6-N was shown to interact with actin (40). It would be of interest to probe whether this region is implicated in MAP6-N association with actin and whether Ca^{2+}-CaM binding to this region may regulate such process.

In conclusion, we report here for the first time structure and functional information on a short region from MAP6 that recapitulates its ability to bind and stabilize MTs upon exposure to cold or nocodazole. The binding of this region to MTs appears modulated by a competitive interaction with Ca^{2+}-CaM, which further documents the complex regulation of MT assembly by MAP6.

Acknowledgments—We thank Rabia Letaief for help with NMR resonance assignment and Imane Hamdi for cell culture experiments. We thank Sylviane Hoos and Patrick England from La Plate-forme de Biophysique des Macromolécules et de leurs Interactions (Institut Pasteur, Paris, France) for help, technical support, and fruitful discussions.

[5] P. Gans, personal communication.

REFERENCES

1. Webb, B. C., and Wilson, L. (1980) Cold-stable microtubules from brain. *Biochemistry* **19,** 1993–2001

2. Baas, P. W., and Heidemann, S. R. (1986) Microtubule reassembly from nucleating fragments during the regrowth of amputated neurites. *J. Cell Biol.* **103,** 917–927
3. Baas, P. W., Slaughter, T., Brown, A., and Black, M. M. (1991) Microtubule dynamics in axons and dendrites. *J. Neurosci. Res.* **30,** 134–153
4. Guillaud, L., Bosc, C., Fourest-Lieuvin, A., Denarier, E., Pirollet, F., Lafanechère, L., and Job, D. (1998) STOP proteins are responsible for the high degree of microtubule stabilization observed in neuronal cells. *J. Cell Biol.* **142,** 167–179
5. Galiano, M. R., Bosc, C., Schweitzer, A., Andrieux, A., Job, D., and Hallak, M. E. (2004) Astrocytes and oligodendrocytes express different STOP protein isoforms. *J. Neurosci. Res.* **78,** 329–337
6. Margolis, R. L., Rauch, C. T., and Job, D. (1986) Purification and assay of a 145-kDa protein (STOP145) with microtubule-stabilizing and motility behavior. *Proc. Natl. Acad. Sci. U.S.A.* **83,** 639–643
7. Margolis, R. L., Rauch, C. T., Pirollet, F., and Job, D. (1990) Specific association of STOP protein with microtubules *in vitro* and with stable microtubules in mitotic spindles of cultured cells. *EMBO J.* **9,** 4095–4102
8. Bosc, C., Cronk, J. D., Pirollet, F., Watterson, D. M., Haiech, J., Job, D., and Margolis, R. L. (1996) Cloning, expression, and properties of the microtubule-stabilizing protein STOP. *Proc. Natl. Acad. Sci. U.S.A.* **93,** 2125–2130
9. Denarier, E., Fourest-Lieuvin, A., Bosc, C., Pirollet, F., Chapel, A., Margolis, R. L., and Job, D. (1998) Nonneuronal isoforms of STOP protein are responsible for microtubule cold stability in mammalian fibroblasts. *Proc. Natl. Acad. Sci. U.S.A.* **95,** 6055–6060
10. Denarier, E., Aguezzoul, M., Jolly, C., Vourc'h, C., Roure, A., Andrieux, A., Bosc, C., and Job, D. (1998) Genomic structure and chromosomal mapping of the mouse STOP gene (Mtap6). *Biochem. Biophys. Res. Commun.* **243,** 791–796
11. Aguezzoul, M., Andrieux, A., and Denarier, E. (2003) Overlap of promoter and coding sequences in the mouse STOP gene (Mtap6). *Genomics* **81,** 623–627
12. Andrieux, A., Salin, P. A., Vernet, M., Kujala, P., Baratier, J., Gory-Fauré, S., Bosc, C., Pointu, H., Proietto, D., Schweitzer, A., Denarier, E., Klumperman, J., and Job, D. (2002) The suppression of brain cold-stable microtubules in mice induces synaptic defects associated with neuroleptic-sensitive behavioral disorders. *Genes Dev.* **16,** 2350–2364
13. Delotterie, D., Ruiz, G., Brocard, J., Schweitzer, A., Roucard, C., Roche, Y., Suaud-Chagny, M. F., Bressand, K., and Andrieux, A. (2010) Chronic administration of atypical antipsychotics improves behavioral and synaptic defects of STOP null mice. *Psychopharmacology* **208,** 131–141
14. Shimizu, H., Iwayama, Y., Yamada, K., Toyota, T., Minabe, Y., Nakamura, K., Nakajima, M., Hattori, E., Mori, N., Osumi, N., and Yoshikawa, T. (2006) Genetic and expression analyses of the STOP (MAP6) gene in schizophrenia. *Schizophr. Res.* **84,** 244–252
15. Choi, K. H., Zepp, M. E., Higgs, B. W., Weickert, C. S., and Webster, M. J. (2009) Expression profiles of schizophrenia susceptibility genes during human prefrontal cortical development. *J. Psychiatry Neurosci.* **34,** 450–458
16. Martins-De-Souza, D., Dias-Neto, E., Schmitt, A., Falkai, P., Gormanns, P., Maccarrone, G., Turck, C. W., and Gattaz, W. F. (2010) Proteome analysis of schizophrenia brain tissue. *World J. Biol. Psychiatry* **11,** 110–120
17. Benardais, K., Kasem, B., Couegnas, A., Samama, B., Fernandez, S., Schaeffer, C., Antal, M. C., Job, D., Schweitzer, A., Andrieux, A., Giersch, A., Nehlig, A., and Boehm, N. (2010) Loss of STOP protein impairs peripheral olfactory neurogenesis. *PLoS One* **5,** e12753
18. Delphin, C., Bouvier, D., Seggio, M., Couriol, E., Saoudi, Y., Denarier, E., Bosc, C., Valiron, O., Bisbal, M., Arnal, I., and Andrieux, A. (2012) MAP6-F is a temperature sensor that directly binds to and protects microtubules from cold-induced depolymerization. *J. Biol. Chem.* **287,** 35127–35138
19. Bosc, C., Frank, R., Denarier, E., Ronjat, M., Schweitzer, A., Wehland, J., and Job, D. (2001) Identification of novel bifunctional calmodulin-binding and microtubule-stabilizing motifs in STOP proteins. *J. Biol. Chem.* **276,** 30904–30913
20. Job, D., Fischer, E. H., and Margolis, R. L. (1981) Rapid disassembly of cold-stable microtubules by calmodulin. *Proc. Natl. Acad. Sci. U.S.A.* **78,** 4679–4682
21. Job, D., Rauch, C. T., Fischer, E. H., and Margolis, R. L. (1982) Recycling of cold-stable microtubules: evidence that cold stability is due to substoichiometric polymer blocks. *Biochemistry* **21,** 509–515
22. Bouvier, D., Vanhaverbeke, C., Simorre, J. P., Arlaud, G. J., Bally, I., Forge, V., Margolis, R. L., Gans, P., and Kleman, J. P. (2003) Unusual Ca^{2+}-calmodulin binding interactions of the microtubule-associated protein F-STOP. *Biochemistry* **42,** 11484–11493
23. Castoldi, M., and Popov, A. V. (2003) Purification of brain tubulin through two cycles of polymerization-depolymerization in a high-molarity buffer. *Protein Expr. Purif.* **32,** 83–88
24. Chernov, K. G., Curmi, P. A., Hamon, L., Mechulam, A., Ovchinnikov, L. P., and Pastré, D. (2008) Atomic force microscopy reveals binding of mRNA to microtubules mediated by two major mRNP proteins YB-1 and PABP. *FEBS Lett.* **582,** 2875–2881
25. Grzesiek, S., and Bax, A. (1993) Amino acid type determination in the sequential assignment procedure of uniformly 13C/15N-enriched proteins. *J. Biomol. NMR* **3,** 185–204
26. Johnson, B. A., and Blevins, R. A. (1994) NMR View: A computer program for the visualization and analysis of NMR data. *J. Biomol. NMR* **4,** 603–614
27. Favier, A., and Brutscher, B. (2011) Recovering lost magnetization: polarization enhancement in biomolecular NMR. *J. Biomol. NMR* **49,** 9–15
28. Delaglio, F., Grzesiek, S., Vuister, G. W., Zhu, G., Pfeifer, J., and Bax, A. (1995) NMRPipe: a multidimensional spectral processing system based on UNIX pipes. *J. Biomol. NMR* **6,** 277–293
29. Humphrey, W., Dalke, A., and Schulten, K. (1996) VMD: visual molecular dynamics. *J. Mol. Graph* **14,** 33–38, 27–28
30. Lieuvin, A., Labbé, J. C., Dorée, M., and Job, D. (1994) Intrinsic microtubule stability in interphase cells. *J. Cell Biol.* **124,** 985–996
31. Chernov, K. G., Mechulam, A., Popova, N. V., Pastre, D., Nadezhdina, E. S., Skabkina, O. V., Shanina, N. A., Vasiliev, V. D., Tarrade, A., Melki, J., Joshi, V., Baconnais, S., Toma, F., Ovchinnikov, L. P., and Curmi, P. A. (2008) YB-1 promotes microtubule assembly *in vitro* through interaction with tubulin and microtubules. *BMC Biochem.* **9,** 23
32. Wishart, D. S., Bigam, C. G., Yao, J., Abildgaard, F., Dyson, H. J., Oldfield, E., Markley, J. L., and Sykes, B. D. (1995) ^{1}H, ^{13}C, and ^{15}N chemical shift referencing in biomolecular NMR. *J. Biomol. NMR* **6,** 135–140
33. Lefèvre, J., Chernov, K. G., Joshi, V., Delga, S., Toma, F., Pastré, D., Curmi, P. A., and Savarin, P. (2011) The C terminus of tubulin, a versatile partner for cationic molecules: binding of Tau, polyamines, and calcium. *J. Biol. Chem.* **286,** 3065–3078
34. Ban, C., Ramakrishnan, B., Ling, K. Y., Kung, C., and Sundaralingam, M. (1994) Structure of the recombinant *Paramecium tetraurelia* calmodulin at 1.68 A resolution. *Acta Crystallogr. D Biol. Crystallogr.* **50,** 50–63
35. Bonnet, C., Denarier, E., Bosc, C., Lazereg, S., Denoulet, P., and Larcher, J. C. (2002) Interaction of STOP with neuronal tubulin is independent of polyglutamylation. *Biochem. Biophys. Res. Commun.* **297,** 787–793
36. Al-Bassam, J., Ozer, R. S., Safer, D., Halpain, S., and Milligan, R. A. (2002) MAP2 and tau bind longitudinally along the outer ridges of microtubule protofilaments. *J. Cell Biol.* **157,** 1187–1196
37. Moores, C. A., Perderiset, M., Francis, F., Chelly, J., Houdusse, A., and Milligan, R. A. (2004) Mechanism of microtubule stabilization by doublecortin. *Mol. Cell* **14,** 833–839
38. Makarov, A. A., Tsvetkov, P. O., Villard, C., Esquieu, D., Pourroy, B., Fahy, J., Braguer, D., Peyrot, V., and Lafitte, D. (2007) Vinflunine, a novel microtubule inhibitor, suppresses calmodulin interaction with the microtubule-associated protein STOP. *Biochemistry* **46,** 14899–14906
39. Kakiuchi, S., and Sobue, K. (1981) Ca^{2+}-and calmodulin-dependent flip-flop mechanism in microtubule assembly-disassembly. *FEBS Lett.* **132,** 141–143
40. Baratier, J., Peris, L., Brocard, J., Gory-Fauré, S., Dufour, F., Bosc, C., Fourest-Lieuvin, A., Blanchoin, L., Salin, P., Job, D., and Andrieux, A. (2006) Phosphorylation of microtubule-associated protein STOP by calmodulin kinase II. *J. Biol. Chem.* **281,** 19561–19569
41. He, L., Hou, Z., and Qi, R. Z. (2008) Calmodulin binding and Cdk5 phosphorylation of p35 regulate its effect on microtubules. *J. Biol. Chem.* **283,** 13252–13260
42. Lee, Y. C., and Wolff, J. (1984) The calmodulin-binding domain on microtubule-associated protein 2. *J. Biol. Chem.* **259,** 8041–8044

43. Kotani, S., Nishida, E., Kumagai, H., and Sakai, H. (1985) Calmodulin inhibits interaction of actin with MAP2 and Tau, two major microtubule-associated proteins. *J. Biol. Chem.* **260,** 10779–10783
44. Padilla, R., Maccioni, R. B., and Avila, J. (1990) Calmodulin binds to a tubulin binding site of the microtubule-associated protein tau. *Mol. Cell Biochem.* **97,** 35–41
45. Meador, W. E., Means, A. R., and Quiocho, F. A. (1993) Modulation of calmodulin plasticity in molecular recognition on the basis of x-ray structures. *Science* **262,** 1718–1721
46. Osawa, M., Tokumitsu, H., Swindells, M. B., Kurihara, H., Orita, M., Shibanuma, T., Furuya, T., and Ikura, M. (1999) A novel target recognition revealed by calmodulin in complex with Ca^{2+}-calmodulin-dependent kinase kinase. *Nat. Struct. Biol.* **6,** 819–824
47. McIlroy, B. K., Walters, J. D., Blackshear, P. J., and Johnson, J. D. (1991) Phosphorylation-dependent binding of a synthetic MARCKS peptide to calmodulin. *J. Biol. Chem.* **266,** 4959–4964
48. Blackshear, P. J. (1993) The MARCKS family of cellular protein kinase C substrates. *J. Biol. Chem.* **268,** 1501–1504
49. Minami, Y., Kawasaki, H., Suzuki, K., and Yahara, I. (1993) The calmodulin-binding domain of the mouse 90-kDa heat shock protein. *J. Biol. Chem.* **268,** 9604–9610
50. Larkin, M. A., Blackshields, G., Brown, N. P., Chenna, R., McGettigan, P. A., McWilliam, H., Valentin, F., Wallace, I. M., Wilm, A., Lopez, R., Thompson, J. D., Gibson, T. J., and Higgins, D. G. (2007) Clustal W and Clustal X version 2.0. *Bioinformatics* **23,** 2947–2948
51. Livingstone, C. D., and Barton, G. J. (1993) Protein sequence alignments: a strategy for the hierarchical analysis of residue conservation. *Comput. Appl. Biosci.* **9,** 745–756
52. Mulder, F. A., Schipper, D., Bott, R., and Boelens, R. (1999) Altered flexibility in the substrate-binding site of related native and engineered high-alkaline *Bacillus* subtilisins. *J. Mol. Biol.* **292,** 111–123